J. Fluid Mech. (1997), *vol.* 350, *pp.* 231–259. Printed in the United Kingdom

The stability of rotating-disc boundary-layer flow over a compliant wall. Part 1. Type I and II instabilities

By A. J. COOPER† AND PETER W. CARPENTER

Department of Engineering, University of Warwick, Coventry, CV4 7AL, UK

(Received 23 May 1996 and in revised form 3 July 1997)

A theoretical study into the effects of wall compliance on the stability of the rotating-disc boundary layer is described. A single-layer viscoelastic wall model is coupled to a sixth-order system of fluid stability equations which take into account the effects of viscosity, Coriolis acceleration, and streamline curvature. The coupled system of equations is integrated numerically by a spectral Chebyshev-tau technique.

Travelling and stationary modes are studied and wall compliance is found to greatly increase the complexity of the eigenmode spectrum. It is effective in stabilizing the inviscid Type I (or cross-flow) instability. The effect on the viscous (Type II) eigenmode is more complex and can be strongly destabilizing. An analysis of the energy flux indicates that this destabilization arises as a result of a large degree of energy production by viscous stresses at the wall/flow interface.

The Type I and II instabilities are shown to be negative and positive energy waves respectively. The co-existence of eigenmodes of opposite energy type indicates the possibility of modal interaction and coalescence. It is found that, compared with the rigid disc, wall compliance promotes the interaction and coalescence of the Type I and II eigenmodes. There is an associated strong instability which appears to be characterized by marked horizontal motion of the compliant surface. Modal coalescence is interpreted physically as producing local algebraic growth which could advance the onset of nonlinear effects.

1. Introduction

It has been clearly established over the last decade, through experimental and theoretical investigations, that wall compliance can suppress the growth of Tollmien–Schlichting (T–S) waves in a flat-plate boundary layer leading to a substantial delay in the onset of laminar-turbulent transition. Reviews are given by Gad-el-Hak (1986), Riley, Gad-el-Hak & Metcalfe (1988) and Carpenter (1990). However, these positive conclusions remain pertinent only to the case of the two-dimensional Blasius boundary layer with zero external pressure gradient where T–S waves become destabilized by an essentially viscous mechanism. It remains to be established whether wall compliance is as effective in controlling the growth of other forms of instability, particularly those arising as a result of inviscid instability mechanisms.

This is an important question since in real aerospace and marine applications

† Present address: Department of Applied Mathematics and Theoretical Physics, University of Cambridge, Silver Street, Cambridge CB3 9EW, UK.

boundary layers are usually three-dimensional and/or develop in a non-zero pressure gradient, which is likely to be adverse over some part of the surface. The instabilities which arise in these cases are of a different nature to the T–S instability. Velocity profiles with points of inflection can develop either because of the effects of an adverse pressure gradient or as a result of the three-dimensional nature of the flow. The presence of an inflection point in the velocity profile promotes the more powerful, inviscid instability mechanism identified by Rayleigh (1880) and in the case of three-dimensional flows the instability manifests itself in the form of cross-flow vortices. The growth of disturbances generated by this mechanism persists to indefinitely high Reynolds number and the amplification rates are also significantly higher than those of the T–S instability. In order for wall compliance to be useful in a practical sense it is therefore desirable that it should be effective in reducing growth rates in cases where this inflection-point instability dominates. It has been established theoretically (Cooper & Carpenter 1997*a*) that wall compliance can act to stabilize such inflection-point instabilities in two-dimensional boundary layers in the presence of an adverse pressure gradient. The aim in this paper is to establish whether wall compliance is capable of controlling instability growth in a three-dimensional boundary layer where inflection-point instability mechanisms dominate.

The representative case examined here is the three-dimensional boundary layer which develops over a rotating disc in an initially still ambient fluid. This relatively simple idealized flow exhibits many of the features found in boundary layers in practical applications. Of significance is the cross-flow instability which arises as a result of an inflection point in the radial component of the velocity profile and it is this form of instability which can lead to transition in the leading-edge region of swept wings. The rotating disc provides a convenient means of studying three-dimensional boundary layers experimentally as well as being amenable to theoretical studies. Recently Cooper & Carpenter (1995) and Carpenter & Cooper (1996) have carried out preliminary stability analyses to study the effects of wall compliance on the three-dimensional boundary layer over a rotating disc. Their results indicate that wall compliance can have a markedly stabilizing effect on the inviscid instability modes. The current paper presents further results from this investigation, focusing attention on stationary Type I disturbances, which have been well-studied in the rigid-disc case, as well as presenting further results concerning the Type II instability.

Although the primary instability mechanism is essentially inviscid, viscous effects must be considered in the stability analysis if growth rates are to be represented accurately. Incorporating viscous terms in the usual sense results in the well-known Orr–Sommerfeld equation. In the case of the rotating disc, however, this fourth-order equation is not sufficient to represent the instability characteristics completely. Lilly (1966) established that the inclusion of Coriolis acceleration terms had a significant effect on the stability characteristics of the Ekman boundary layer owing to the generation of the Type II instability. Later Malik, Wilkinson & Orszag (1981) demonstrated that Coriolis and streamline curvature effects also have a significant stabilizing effect on the stationary Type I disturbances for the rotating-disc boundary layer. Incorporating both of these effects results in a sixth-order system of ordinary differential equations which reduces to the Orr–Sommerfeld equation when the Coriolis and streamline curvature terms are neglected.

The instability of the boundary layer over a rigid rotating disc has been studied extensively and the characteristic features of the eigenmode spectrum are quite complex: at least three distinct families of eigensolutions have been identified. One is the inviscid or Type I instability first studied by Gregory, Stuart & Walker (1955)

which was followed by notable contributions from Malik *et al.* (1981), Wilkinson & Malik (1983, 1985) and Mack (1985). This form of instability is considered to be the commonest route to transition and has been well studied experimentally. The early work by Gregory *et al.* using a china-clay visualization technique was able to show the cross-flow instability clearly, which appeared as a series of closely spaced spiral streaks stationary relative to the disc surface. Mack successfully modelled theoretically the modulated disturbance forms observed experimentally by Wilkinson & Malik, thereby establishing that they result from a superposition of the complete zero-frequency azimuthal wavenumber spectrum. It was also noted by Mack (1985) that, although the experimentally observed spiral streaks correspond to zero-frequency disturbances, they are not the most unstable modes in the boundary layer. Some travelling modes were found to have a higher growth rate than the stationary ones. More comprehensive information on the theoretical stability characteristics of travelling modes was supplied by Balakumar & Malik (1990) who confirmed Mack's results.

Until fairly recently the role of the travelling disturbances in experiments on transition remained fairly obscure. This was despite the fact that in the first experimental study of instability of the rotating-disc boundary layer Smith (1946) used two hot-wire probes and detected travelling disturbances. Recently, however, travelling modes have been detected and studied experimentally. Jarre, Le Gal & Chauve (1996*a*, *b*) (see also Jarre, Le Gal & Chauve 1991 and Le Gal 1992) have carried out two-point measurements with hot-film probes enabling them to measure phase speeds. Jarre *et al.* (1996*a*) found that, for the natural transition process over a nominally smooth disc, travelling waves dominated in the early stages of instability. For the later stages, when the disturbances had reached a larger amplitude, stationary disturbances dominated. Jarre *et al.* (1996*b*) then studied the case when transition is forced with a roughness element placed at a position just inboard of the location corresponding to the linear threshold for Type I instability. The roughness element was of a size comparable to the boundary-layer thickness and accordingly generated fairly strong finite-amplitude disturbances. Nevertheless one might have expected strong stationary disturbances to have dominated the transition process. What was found instead was that the dominant disturbances had a small, but definite, negative phase speed, i.e. they travelled with a circumferential phase speed slightly less than the disc rotation speed. The range of propagation angles at this phase speed agreed well with the theoretical predictions of Balakumar & Malik (1990). But, owing to finite-amplitude effects, good agreement with linear stability theory was not found in other respects. It is probably true, however, that the most dramatic role played by the travelling modes is to generate absolute instability. This was discovered recently by Lingwood (1995, 1996) and will be discussed below. Corke & Knasiak (1996) appear to have discovered another important role played by the travelling modes in the transition process and their work will also be discussed below.

A second family of eigenmodes, termed Type II, contains a weaker, viscous instability which appears only when Coriolis effects are included. A similar instability was first discovered in the Ekman boundary layer by Faller (1963). In the rotating-disc boundary layer, according to theory, the stationary form of this instability appears at a substantially higher critical Reynolds number than the Type I. This may be why it has not been observed in the great majority of experimental studies. The travelling form of the Type II instability, on the other hand, typically first occurs at a much lower Reynolds numbers than the Type I mode (Balakumar & Malik 1990; Faller 1991). Coriolis acceleration is essential for its destabilization, but little else is known

about the precise physical instability mechanism. The role of the Type II mode in the transition process has been addressed by the numerical study of Faller (1991), but little else is known about this issue.

A third family of eigenmodes, which we will term Type III, was first identified by Mack (1985) and briefly mentioned by Balakumar & Malik (1990). The eigenmodes are found to have relatively large negative values of α_i (where $\alpha = \alpha_r + \mathrm{i}\alpha_i$ is the complex radial wavenumber), but are conventionally considered to be strongly stable modes in view of their inwardly directed group velocity. Recently Lingwood (1995) has shown that the Types III and I eigenmodes can coalesce to form an absolute instability, thereby providing another route to transition. This has been confirmed experimentally in Lingwood (1996). We will investigate the effect of wall compliance on this absolute instability in Part 2 (Cooper & Carpenter 1997*b*).

Hall (1986) has developed triple-deck asymptotic analyses for both the stationary Type I and II instabilities. His linear analysis was the basis for the weakly nonlinear theory of MacKerrell (1987) for the Type II instability. She showed that unless a certain threshold amplitude is exceeded the Type II disturbance will only grow for Reynolds numbers slightly above critical before decaying to zero at higher Reynolds numbers. Clear evidence of the existence of Type II instabilities in the related Ekman boundary-layer flow has long been available (Faller 1963, 1991). MacKerrell's nonlinear theory may partly explain, why, aside from the rather uncertain observations of Federov *et al.* (1976), the Type II instability has apparently been much more difficult to identify in experiments on the rotating disc. However, clear evidence of the existence of Type II instabilities has been revealed by Lingwood (1996) in her recent experimental study of the impulsively perturbed rotating-disc flow.

There have been some further studies of nonlinear instability of the rotating-disc system. For example, Bassom & Gajjar (1988) carried out an asymptotic study along broadly similar lines to Hall (1986) and MacKerrell (1987) for weakly and strongly nonlinear non-stationary instabilities. Of course, nonlinear mechanisms in some form must be responsible for the final breakdown to turbulence. The most widely studied such mechanism is the secondary instability of the Type I mode. It was evident in the hot-wire signals of Wilkinson & Malik (1983, 1985). It has been studied experimentally in detail by Kohama (1984, 1987) and Kohama & Suda (1993) and theoretically by Balachandar, Streett & Malik (1992) by means of a Floquet analysis. More recently Corke & Knasiak (1996) have shown that a triad coupling between pairs of travelling eigenmodes and a stationary mode could be responsible for the final breakdown to turbulence in their experimental study.

A series of experimental studies has been carried out on the rotating disc with a compliant wall by Hansen & Hunston (1974, 1976, 1983) who used polyvinyl-chloride walls. Their work focused on hydroelastic instability. The experimental study of Chung (1985), who used walls of a multi-layered construction, found drag reduction in some cases. This suggests that either transition delay or turbulence reduction occurred. But the drag reduction was detected solely by torque measurements, so the physical mechanisms responsible could not be determined.

Compliant-wall dynamics can be represented theoretically by using the plate–spring model of Carpenter & Garrad (1985). This model is relatively simple to implement computationally but in order to relate to ongoing experimental investigations the more realistic volume-based compliant-wall model described by Yeo (1988) and Dixon, Lucey & Carpenter (1994) is used in the present paper. This type of wall basically comprises a soft viscoelastic substrate layer firmly attached at the base to a rigid wall with or without a much stiffer thin outer layer. Recently Yeo, Khoo &

Chong (1994*a*) have investigated the so-called non-parallel effects on boundary-layer stability over compliant walls of this type.

The effects of wall compliance as far as controlling flow instabilities is concerned obviously increase with the degree of compliance, but the walls are themselves wave-bearing media and above some threshold level become susceptible to wall-based instabilities. These instabilities can provide an alternative route to transition. They can also generate powerful instabilities through modal coalescence. There are two principal hydroelastic modes, namely divergence and travelling-wave flutter (TWF) which generally limit the admissible degree of compliance.

The divergence instability can be particularly damaging to the prospects of using wall compliance as an effective means of transition delay. It is induced by an imbalance between the wall's structural forces and the conservative hydrodynamic pressure forces generated by disturbances on the surface. Divergence has been shown to be an absolute instability such that disturbance kinetic energy is not convected away from its point of origin and grows indefinitely at that location. It is therefore essential that any compliant wall used for laminar-flow control should be free from this instability.

TWF is a convective instability but brought about by an essentially inviscid mechanism. It is characterized by high phase speeds close to the free-stream value and this instability grows by the irreversible transfer of energy from the flow to the wall as a result of work done by the fluctuating pressure. This hydroelastic mode can persist to indefinitely high Reynolds number and Lucey & Carpenter (1995) show that TWF is a common route to transition in the boundary layers over compliant walls studied experimentally by Gaster (1987). Wall parameters should therefore be chosen carefully to avoid both divergence and TWF.

In order for wall compliance to be most effective wall parameters would ideally be selected to give marginal stability with respect to the wall-based instabilities. However, when using the realistic viscoelastic wall model in conjunction with the three-dimensional geometry of the disc it would be difficult and computationally costly to determine such optimal wall parameters. Our experimental and theoretical investigations for the rotating disc are therefore restricted to compliant walls of single-layer construction. This type of wall is also somewhat easier to manufacture than the two-layer configuration. Despite the apparent simplicity of the single-layer wall it has been observed for the two-dimensional Blasius boundary layer that the eigenvalue spectrum for the coupled wall/flow problem exhibits considerable complexity. Yeo (1988) established numerically the existence of at least four different unstable eigenmodes for Blasius flow over a single-layer viscoelastic wall. The instabilities which develop in this wall/flow configuration were also investigated by Fraser & Carpenter (1985) with the observation that in the absence of any flow there exists an infinite number of free wave modes and that at least the first three of these may develop into instabilities.

In the present paper, Part 1, attention is focused on the response of the Type I and II modes to the presence of a compliant boundary. The effect of wall compliance on the absolute instability of the rotating-disc boundary layer, arising from the coalescence of the Type I and III eigenmodes, is considered in Part 2 (Cooper & Carpenter 1997*b*). And the hydroelastic instabilities are briefly mentioned in Carpenter & Cooper (1996).

The outline of the paper is as follows. Section 2 describes the formulation of the fluid problem and the numerical method of solution of the governing stability equations. The dynamics of the wall motion and the coupling of wall and fluid motions are described in §3 and §4 respectively. Results from the study are presented

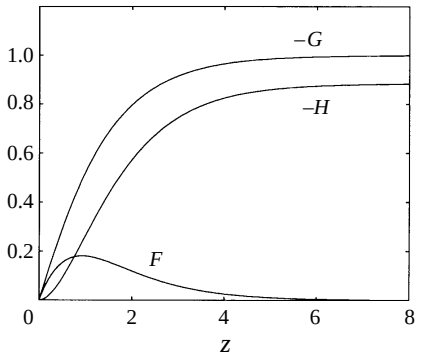

FIGURE 1. Radial (F), azimuthal (G) and axial (H) velocity components for boundary layer flow over a rotating disc.

in §5 where stationary and travelling modes are considered along with an integral energy equation for three-dimensional disturbances. Conclusions are drawn in §6.

2. Formulation of the fluid problem

The disc is assumed to be infinite in diameter and rotating about its centre at a constant angular velocity Ω. A cylindrical coordinate system in the rotating frame is used with radius r^*, azimuthal angle θ and normal direction z^* and the fluid is assumed to occupy the region $z^* > 0$. The mean flow field is obtained from the exact similarity solution of the Navier–Stokes equations due to von Kármán (1921). In the rotating frame the mean velocity components and pressure are written

$$\bar{u} = r^*\Omega F(z), \qquad \bar{v} = r^*\Omega G(z),$$
$$\bar{w} = (\nu\Omega)^{1/2} H(z), \qquad \bar{p} = \rho\nu\Omega P(z),$$

where z is the non-dimensional length scaled by the boundary-layer displacement thickness $\delta^* = (\nu/\Omega)^{1/2}$, with ν the kinematic viscosity and ρ the fluid density.

Using these expressions in the Navier–Stokes equations gives the following governing conditions for the mean flow field where primes denote differentiation with respect to z:

$$F^2 - (G+1)^2 + F'H - F'' = 0, \tag{1}$$
$$2F(G+1) + G'H - G'' = 0, \tag{2}$$
$$P' + HH' - H'' = 0, \tag{3}$$
$$2F + H' = 0. \tag{4}$$

Boundary conditions are

$$F(0) = G(0) = H(0) = 0,$$
$$F = 0, \qquad G = -1 \qquad \text{as} \qquad z \to \infty.$$

The variation of the non-dimensional mean velocity components, F, G and H with z are shown in figure 1.

A linear stability analysis, following Malik *et al.* (1981), is carried out first for the rigid-wall problem, whilst the adaptation of this to incorporate a compliant boundary will be treated in a subsequent section.

A space–time-dependent perturbation field of infinitesimal disturbances, $[\tilde{\boldsymbol{u}}, \tilde{p}]$, is

imposed on the mean flow field, and throughout δ^*, $r_e^*\Omega$ and $\rho r_e^{*2}\Omega^2$ are used to non-dimensionalize length, velocity and pressure respectively with r_e^* taken to be a fixed radial position for the stability analysis. This gives the following dimensionless form for the perturbed flow field:

$$u(r,\theta,z,t) = \frac{r}{R}F(z) + \tilde{u}(r,\theta,z,t), \tag{5}$$

$$v(r,\theta,z,t) = \frac{r}{R}G(z) + \tilde{v}(r,\theta,z,t), \tag{6}$$

$$w(r,\theta,z,t) = \frac{1}{R}H(z) + \tilde{w}(r,\theta,z,t), \tag{7}$$

$$p(r,\theta,z,t) = \frac{1}{R^2}P(z) + \tilde{p}(r,\theta,z,t). \tag{8}$$

$r = r^*(\Omega/\nu)^{1/2}$ is the variable non-dimensional radius and the Reynolds number

$$R = r_e^*(\Omega/\nu)^{1/2}$$

is the non-dimensional fixed radius.

The non-dimensional Navier–Stokes equations for this flow problem in the rotating frame are

$$\frac{\partial \boldsymbol{u}}{\partial t} + (\boldsymbol{u}\cdot\nabla)\boldsymbol{u} + \frac{2}{R}(\boldsymbol{k}\wedge\boldsymbol{u}) + \nabla p - \frac{1}{R}\nabla^2\boldsymbol{u} = 0, \tag{9}$$

$$\nabla\cdot\boldsymbol{u} = 0, \tag{10}$$

where $\boldsymbol{u} = [u,v,w]^T$ and $\boldsymbol{k}$ is the unit vector in the z-direction. $(2/R)\boldsymbol{k}\wedge\boldsymbol{u}$ is the Coriolis acceleration whilst centrifugal terms have been incorporated within a modified pressure term, p.

The above equations are linearized with respect to the disturbances and following this several approximations are made which allow the equations to become separable in r, θ and t. Firstly the quantity r is replaced by R so that the slow variation of flow variables with r is ignored. Terms of order R^{-2} and higher-order terms are subsequently assumed to be negligible. The perturbation quantities are then expressed in the form of normal modes so that

$$[\tilde{u},\tilde{v},\tilde{w},\tilde{p}]^T = [f(z),g(z),h(z),\pi(z)]^T E + \text{c.c.} \tag{11}$$

where $E = \exp\{\mathrm{i}(\alpha r + \beta R\theta - \omega t)\}$, α is the radial wavenumber, β the azimuthal wavenumber, ω the frequency of the disturbance and c.c denotes complex conjugate. All quantities are dimensionless. Strictly βR should be an integer to ensure that $E(\theta + 2\pi) = E(\theta)$. It is typically much greater than 1. Accordingly, along with most other authors, we treat β as continuously varying for the purposes of graphical presentation.

Substitution of disturbance form (11) into the linearized equations followed by the introduction of a new variable, $\gamma = \alpha g - \beta f$, allows pressure terms to be eliminated leaving two coupled equations:

$$\Big[\mathrm{i}(\mathrm{D}^2-\lambda^2)(\mathrm{D}^2-\bar{\lambda}^2)+R(\alpha F+\beta G-\omega)(\mathrm{D}^2-\bar{\lambda}^2)-R(\bar{\alpha}F''+\beta G'') - \mathrm{i}H\mathrm{D}(\mathrm{D}^2-\bar{\lambda}^2) - \mathrm{i}H'(\mathrm{D}^2-\bar{\lambda}^2) - \mathrm{i}F\mathrm{D}^2\Big]h + \Big[2(G+1)\mathrm{D} + 2G'\Big]\gamma = 0, \tag{12}$$

$$\Big[2(G+1)\mathrm{D}-\mathrm{i}R(\alpha G'-\beta F')\Big]h + \Big[\mathrm{i}(\mathrm{D}^2-\lambda^2)+R(\alpha F+\beta G-\omega)-\mathrm{i}H\mathrm{D}-\mathrm{i}F\Big]\gamma = 0, \tag{13}$$

where $\mathrm{D} \equiv \mathrm{d}/\mathrm{d}z$, $\bar{\alpha} = \alpha - \mathrm{i}/R$, $\lambda^2 = \alpha^2 + \beta^2$ and $\bar{\lambda}^2 = \alpha\bar{\alpha} + \beta^2$.

The boundary conditions corresponding to this coupled system for the rigid boundary are

$$h(0) = h'(0) = \gamma(0) = 0,$$

$$h(\infty) = h'(\infty) = \gamma(\infty) = 0.$$

This sixth-order system of equations, as originally derived by Malik *et al.* (1981), retains the effects of Coriolis acceleration and streamline curvature and defines an eigenvalue problem of the form

$$\mathscr{F}(\alpha; \beta, \omega, R) = 0.$$

The most appropriate physical interpretation for this eigenvalue problem is to consider spatial modes where the frequency, ω, is real and following Mack (1985) it is assumed that the amplitude distribution is axisymmetric with $\beta_i = 0$. The eigenvalue relation thus determines the complex wavenumber, $\alpha = \alpha_r + \mathrm{i}\alpha_i$, with the local spatial growth rate given by $-\alpha_i$ when the disturbances propagate outwards.

2.1. *Numerical solution of the stability equations*

The sixth-order system of equations is solved numerically using a Chebyshev-tau spectral method, chosen because of its computational efficiency and accuracy. The general Chebyshev-tau formulation also allows a global eigenvalue search scheme to be implemented for the rigid wall which enables all solution branches to be identified. Malik *et al.* (1981) used a similar spectral scheme. They solved for the temporal case which reduces the size of the computational problem, but involved the use of a group velocity transformation to obtain spatial eigenvalues, whereas we solve directly for the spatial eigenvalues.

The numerical scheme begins by transforming the physical space ($z \in [0, \infty]$) to the computational domain ($y \in [-1, 1]$) using the transformation

$$y = \frac{z-2}{z+2}. \tag{14}$$

The system of equations, (12) and (13), written in terms of the computational variable can be expressed in the form

$$\tilde{A}h + \tilde{B}h' + \tilde{C}h'' + \tilde{D}h''' + \tilde{E}h^{\mathrm{iv}} + \tilde{F}\gamma + \tilde{G}\gamma' = 0, \tag{15}$$

$$\tilde{V}h + \tilde{W}h' + \tilde{X}\gamma + \tilde{Y}\gamma' + \tilde{Z}\gamma'' = 0, \tag{16}$$

where primes now denote derivatives with respect to y and the coefficients $\tilde{A}$ etc. follow from (12) and (13). Equation (15) is then integrated indefinitely four times and (16) twice to give

$$\begin{aligned}\iiiint(\tilde{A} - \tilde{B}' + \tilde{C}'' - \tilde{D}''' + \tilde{E}^{\mathrm{iv}})h\,\mathrm{d}y + \iiint(\tilde{B} - 2\tilde{C}' + 3\tilde{D}'' - 4\tilde{E}''')h\,\mathrm{d}y \\ + \iint(\tilde{C} - 3\tilde{D}' + 6\tilde{E}'')h\,\mathrm{d}y + \int(\tilde{D} - 4\tilde{E}')h\,\mathrm{d}y + \tilde{E}h \\ + \iiiint(\tilde{F} - \tilde{G}')\gamma\,\mathrm{d}y + \iiint\tilde{G}\gamma\,\mathrm{d}y = d_0 + d_1 y + d_2 y^2 + d_3 y^3,\end{aligned} \tag{17}$$

$$\begin{aligned}\iint(\tilde{V} - \tilde{W}')h\,\mathrm{d}y + \int\tilde{W}h\,\mathrm{d}y + \int(\tilde{Y} - 2\tilde{Z}')\gamma\,\mathrm{d}y \\ + \iint(\tilde{X} - \tilde{Y}' + \tilde{Z}'')\gamma\,\mathrm{d}y + \tilde{Z}\gamma = e_0 + e_1 y,\end{aligned} \tag{18}$$

where the d_i and e_i are constants of integration.

The working variables h and γ, in terms of the transformed coordinate, are then written as two finite Chebyshev series expansions:

$$h = \sum_{n=0}^{N} a_n T_n(y), \qquad \gamma = \sum_{n=0}^{N} b_n T_n(y). \tag{19}$$

This approximation allows the integrated equations to be discretized and generates $2N + 2$ equations in terms of the unknowns $a_0, \ldots, a_N, b_0, \ldots, b_N$.

The problem is fully specified by the inclusion of six boundary conditions which replace the equations for $n = 0, \ldots, 3$ and $n = 0, 1$ in the first and second discretized equations respectively. The justification for this comes from the fact that these equations serve only to identify the integration constants d_i and e_i.

The equations are then cast in the form

$$\boldsymbol{D}(\alpha) \begin{bmatrix} \boldsymbol{a} \\ \boldsymbol{b} \end{bmatrix} = 0, \tag{20}$$

where $\boldsymbol{D}$ is a square matrix of order $2N + 2$, $\boldsymbol{a} = [a_0, \ldots, a_N]^T$ and $\boldsymbol{b} = [b_0, \ldots, b_N]^T$.

Using the technique of Bridges & Morris (1984) eigenvalues, α, can be obtained iteratively from an initial estimate using the formula

$$\alpha_{k+1} = \alpha_k - \frac{1}{f(\alpha_k)}, \qquad k = 0, 1, \ldots \tag{21}$$

where $f(\alpha_k) = \mathrm{Tr}\{\boldsymbol{D}^{-1}(\alpha_k)\boldsymbol{D}^{(1)}(\alpha_k)\}$ and $\mathrm{Tr}\{\boldsymbol{A}\}$ denotes the trace of matrix $\boldsymbol{A}$; $\boldsymbol{D}^{-1}(\alpha_k)$ is the inverse of $\boldsymbol{D}(\alpha_k)$ and $\boldsymbol{D}^{(1)}(\alpha_k)$ the first derivative of $\boldsymbol{D}(\alpha_k)$ with respect to α.

3. Wall motion

In order to reduce the number of possible wall parameters the single-layer compliant wall chosen for this investigation is assumed to be of infinite depth. This assumption is reasonable since in practice the disturbances in the boundary layer attenuate as they propagate down into the wall and only penetrate to a finite depth. The propagation of disturbances into the wall will be quantified below in §5.3 where the validity of the infinite-depth assumption will be briefly discussed.

It is necessary to solve for the wall and fluid motion separately in the presence of a compliant boundary and then couple the two governing sets of equations through appropriate dynamic and kinematic conditions at the wall/flow interface. The wall dynamics are described by the Navier equations so that the three-dimensional dimensionless displacement vector, $\boldsymbol{\eta} = [\xi, \eta, \zeta]^T$, is governed by the following vector equation:

$$\ddot{\boldsymbol{\eta}} = \frac{\rho}{\rho_s}\left(G_s \nabla^2 \boldsymbol{\eta} + Y_s \nabla\nabla \cdot \boldsymbol{\eta}\right) \tag{22}$$

where G_s and K_s are respectively the dimensionless shear and bulk moduli of the substrate material, ρ_s and ρ are respectively the densities of the substrate and fluid, and $Y_s = K_s + G_s/3$. Throughout a Poisson ratio of 0.49 is used, so that the material is almost incompressible, which generates the relation $K_s = 149G_s/3$. Although this choice is somewhat arbitrary, it can be justified by the fact that the solutions obtained are little different for any other choice of Poisson ratio near 0.5. Wall damping can be included through a complex shear modulus

$$G_s = G_s^R(1 - \mathrm{i}\gamma_s),$$

where γ_s is a real damping coefficient. In the absence of wall damping the material can be assumed to be purely elastic.

There is no clearly defined manner in which to express non-dimensional shear and bulk moduli which are invariant across the disc, since the obvious reference velocity of $r_e^*\Omega$ implies that the effective free-stream speed changes with radial location. The theoretical problem is therefore considered from a practical viewpoint where a layer of fixed material property is used and changes in wall compliance are effected by varying the rotational speed of the disc. Accordingly, an essentially arbitrary choice can be made for the elastic modulus of the material. To retain some correspondence with an ongoing experimental research project, all calculations use a dimensional value of $G_s = 1000\ \mathrm{N\,m^{-2}}$. Note, though, that the effective wall compliance increases as the linear speed, $r_e^*\Omega$, and therefore Reynolds number rises Since the rotating-disc boundary layer is of constant thickness lengths in the wall equations can be non-dimensionalized with respect to the boundary-layer displacement thickness.

The standard travelling-wave form is assumed for the non-dimensional displacement field in response to disturbances within the boundary layer:

$$\boldsymbol{\eta} = [\hat{\xi}(z), \hat{\eta}(z), \hat{\zeta}(z)]^T \exp\{\mathrm{i}(\alpha r + \beta R\theta - \omega t)\} + \text{c.c.} \tag{23}$$

Substitution into the Navier equations then gives:

$$\hat{\xi}'' = -\frac{1}{G_s}[G_s F_s + \mathrm{i}\alpha Y_s \tilde{\alpha}]\hat{\xi} - \frac{\mathrm{i}\alpha Y_s}{G_s}\hat{\zeta}' + \frac{1}{G_s}[\alpha\beta Y_s - 2\beta^2 G_s]\hat{\eta}, \tag{24}$$

$$\hat{\eta}'' = -\frac{1}{G_s}[G_s F_s - \beta^2 Y_s]\hat{\eta} - \frac{\mathrm{i}\beta Y_s}{G_s}\hat{\zeta}' - \frac{1}{G_s}\left[\frac{2\mathrm{i}\beta G_s}{R} + \mathrm{i}\beta Y_s \tilde{\alpha}\right]\hat{\xi}, \tag{25}$$

$$\hat{\zeta}'' = -\frac{1}{(G_s + Y_s)}[G_s F_s \hat{\zeta} + Y_s \tilde{\alpha}\hat{\xi}' + \mathrm{i}\beta Y_s \hat{\eta}'], \tag{26}$$

with $F_s = \mathrm{i}\alpha/R - \alpha^2 - \beta^2 + \rho_s\omega^2/(\rho G_s)$ and $\tilde{\alpha} = 1/R + \mathrm{i}\alpha$. Both the fluid and solid densities are assumed to take the value $1000\ \mathrm{kg\,m^{-3}}$.

Equations (24)–(26) can be written as

$$\tilde{\boldsymbol{\eta}}' = \boldsymbol{K}\tilde{\boldsymbol{\eta}}, \tag{27}$$

where $\tilde{\boldsymbol{\eta}} = [\hat{\xi}', \hat{\eta}', \hat{\zeta}', \hat{\xi}, \hat{\eta}, \hat{\zeta}]^T$ and $\boldsymbol{K}$ takes the form

$$\boldsymbol{K} = \begin{bmatrix} 0 & 0 & k_{13} & k_{14} & k_{15} & 0 \\ 0 & 0 & k_{23} & k_{24} & k_{25} & 0 \\ k_{31} & k_{32} & 0 & 0 & 0 & k_{36} \\ 1 & 0 & 0 & 0 & 0 & 0 \\ 0 & 1 & 0 & 0 & 0 & 0 \\ 0 & 0 & 1 & 0 & 0 & 0 \end{bmatrix}.$$

Six eigenvalues, $\pm\mu_i, i = 1, 2, 3$, are obtained by solving $\det(\boldsymbol{K} - \mu\boldsymbol{I}) = 0$, where $\boldsymbol{I}$ is the identity matrix. A general solution of the following form then results:

$$\begin{bmatrix} \hat{\xi}(z) \\ \hat{\eta}(z) \\ \hat{\zeta}(z) \end{bmatrix} = \sum_{i=1}^{3} \begin{bmatrix} A_i \\ B_i \\ C_i \end{bmatrix} \mathrm{e}^{\mu_i z} + \sum_{i=1}^{3} \begin{bmatrix} \bar{A}_i \\ \bar{B}_i \\ \bar{C}_i \end{bmatrix} \mathrm{e}^{-\mu_i z}, \tag{28}$$

where $A_i, B_i, C_i, \bar{A}_i, \bar{B}_i$ and $\bar{C}_i$ are constants of integration. For an infinitely deep layer $\bar{A}_i, \bar{B}_i$ and $\bar{C}_i$ must be zero in order to satisfy the requirement of zero displacement at

infinite depth and the remaining constants are related through (24)–(26). Substitution of the solutions into (24) and some rearrangement gives

$$B_i = \frac{(\mu_i^2 - k_{14})A_i - k_{13}\mu_i C_i}{k_{15}}. \tag{29}$$

Equation (25) can then be used to eliminate the B_i:

$$\mu_i^2 B_i = k_{24}A_i + k_{25}B_i + k_{23}\mu_i C_i \tag{30}$$

to give

$$A_i = \Phi(\mu_i)C_i, \qquad B_i = \Psi(\mu_i)C_i, \tag{31}$$

where

$$\Phi(\mu_i) = \frac{[k_{23}k_{15}\mu_i + k_{13}\mu_i(\mu_i^2 - k_{25})]}{[\mu_i^4 - \mu_i^2(k_{14} + k_{25}) + k_{25}k_{14} - k_{24}k_{15}]}, \tag{32}$$

$$\Psi(\mu_i) = \frac{(\mu_i^2 - k_{14})\Phi(\mu_i) - k_{13}\mu_i}{k_{15}}. \tag{33}$$

This results in a solution for the displacement vector field in terms of three unknown constants of integration, C_i:

$$\begin{bmatrix} \hat{\xi}(z) \\ \hat{\eta}(z) \\ \hat{\zeta}(z) \end{bmatrix} = \sum_{i=1}^{3} \begin{bmatrix} \Phi(\mu_i) \\ \Psi(\mu_i) \\ 1 \end{bmatrix} C_i e^{\mu_i z}. \tag{34}$$

Inclusion of $1/R$ terms in the wall equations gives rise to non-zero imaginary parts for the free-wave eigenvalues (calculated by assuming a stress-free wall boundary) compared to zero values in any corresponding two-dimensional calculation. These free-wave modes neither decay nor grow if considered in terms of energy transfer and the appearance of positive values for α_i is merely a consequence of the three-dimensional geometry. The apparent decay of these modes can be attributed to the pulse of energy which excites them spreading out radially. (It can be shown from considerations of energy flux that for a purely radial wave $\alpha_i = 1/2R$ which is indeed verified in the numerical results.) In order to correlate with the fluid stability problem, where $\alpha_i = 0$ denotes the boundary between stability and instability, terms of order R^{-1} and smaller are neglected in the wall formulation. This can be thought of as being analogous to ignoring 'non-parallel' effects in the flow.

4. Coupling fluid and wall equations

For the coupled fluid/compliant wall problem boundary conditions are derived by satisfying the conditions of velocity and stress continuity at the wall/flow interface.

Linearized boundary conditions for the three-dimensional velocity profile at the interface are

$$-\mathrm{i}\omega\hat{\xi} = f + F'(0)\hat{\zeta}, \tag{35}$$

$$-\mathrm{i}\omega\hat{\eta} = g + G'(0)\hat{\zeta}, \tag{36}$$

$$-\mathrm{i}\omega\hat{\zeta} = h. \tag{37}$$

Continuity of stress is satisfied by applying the relation

$$\bar{\sigma}_{wall}(r,\theta,0) = \bar{\sigma}_{fluid}(r,\theta,0) + \hat{\zeta}\frac{\partial}{\partial z}[\bar{\sigma}^M](r,\theta,0),$$

where M denotes the mean stress contribution. Therefore at $z = 0$

$$\bar{\sigma}_{zr} = G_s[\mathrm{i}\alpha\hat{\zeta} + \hat{\xi}'] = \frac{1}{R}[\mathrm{i}\alpha h + f'] + \frac{\hat{\zeta}}{R}\frac{\partial}{\partial z}\left[\frac{1}{R}\frac{\partial H}{\partial r}(0) + F'(0)\right]$$
$$= \frac{1}{R}[F''(0)\hat{\zeta} + \mathrm{i}\alpha h + f'], \tag{38}$$

$$\bar{\sigma}_{z\theta} = G_s[\mathrm{i}\beta\hat{\zeta} + \hat{\eta}'] = \frac{1}{R}[\mathrm{i}\beta h + g'] + \frac{\hat{\zeta}}{R}\frac{\partial}{\partial z}\left[\frac{1}{R^2}\frac{\partial H}{\partial \theta}(0) + G'(0)\right]$$
$$= \frac{1}{R}[G''(0)\hat{\zeta} + \mathrm{i}\beta h + g'], \tag{39}$$

$$\bar{\sigma}_{zz} = Y_s[\mathrm{i}\alpha\hat{\xi} + \mathrm{i}\beta\hat{\eta} + \hat{\zeta}'] + 2G_s\hat{\zeta}' = -\pi + \frac{2h'}{R} + \hat{\zeta}\frac{\partial}{\partial z}\left[-\frac{P(0)}{R^2} + \frac{2H'(0)}{R^2}\right]$$
$$= -\pi + \frac{2h'}{R} + O\left(\frac{1}{R^2}\right). \tag{40}$$

An expression for the pressure term π at the mean undisturbed wall position is obtained from the radial momentum equation such that

$$\pi(0) = \frac{1}{R}\left[f'' - \lambda^2 f + 2g\right] + \mathrm{i}\omega f - F'(0)h, \tag{41}$$

which can be rewritten in terms of h and γ through the use of the continuity equation.

Transformation to the computational domain allows the coupling conditions to be expressed in the form of two matrix equations:†

$$[\hat{\xi}, \hat{\eta}, \hat{\zeta}]_w^T = [\boldsymbol{R}]\boldsymbol{C} = [\boldsymbol{S}]\boldsymbol{H}, \tag{42}$$

$$[\bar{\sigma}_{zr}, \bar{\sigma}_{z\theta}, \bar{\sigma}_{zz}]_w^T = [\boldsymbol{X}]\boldsymbol{C} = [\boldsymbol{Y}]\boldsymbol{H}, \tag{43}$$

where $\boldsymbol{C} = [C_1, C_2, C_3]^T$ and $\boldsymbol{H} = [h''', h'', h', h, \gamma'', \gamma', \gamma]_w^T$ (suffix w indicates evaluation at the wall/flow interface.) and $\boldsymbol{R}, \boldsymbol{S}, \boldsymbol{X}$ and $\boldsymbol{Y}$ are complex matrices. Elimination of the unknown vector $\boldsymbol{C}$ then gives rise to three conditions which replace the wall conditions of the rigid boundary problem:

$$[\boldsymbol{R}^{-1}\boldsymbol{S} - \boldsymbol{X}^{-1}\boldsymbol{Y}]\boldsymbol{H} = [0, 0, 0]^T. \tag{44}$$

Centrifugal forces arising as a result of system rotation are expected, in practice, to exert some influence on the compliant wall, causing it to undergo a certain amount of displacement, even in the absence of any boundary-layer disturbances. This may result in some form of 'bulging' at the edges. In the present theoretical calculations, where the disc is assumed to be infinite in extent, edge effects are not included in the problem formulation and this effect is neglected. The significant radial variation in the mean pressure may also affect the degree of compliance slightly as a result of interaction between the perturbation and mean pressure fields in the wall. This was demonstrated theoretically by Yeo, Khoo & Chong (1994*b*) who show that a sufficiently large mean pressure field can significantly affect the stability characteristics of a two-dimensional boundary layer over a compliant wall. With the present linear wall model such effects cannot be modelled.

† A slightly different formulation is used when considering stationary disturbances.

4.1. *Validation of rotating disc/compliant wall code*

Since there are no existing results on this stability problem to compare with our results, a number of tests have been carried out in order to establish that our code was working correctly. The rigid-wall stability characteristics for stationary disturbances have been well-documented (Mack 1985; Malik 1986) and good agreement has been obtained between our results and theirs. The first test was to confirm, by increasing the value of N, that the code converged sufficiently well. Convergence on eigenvalues was achieved to an acceptable degree of tolerance for $N = 56$ compared to a value of $N = 40$ for the rigid-wall code. This is generally the case for compliant wall problems where greater variation occurs in the near-wall region requiring increased resolution to give the same degree of accuracy. The second check for the compliant-wall problem was to take the limiting value of the wall parameter which renders the boundary equivalent to a rigid wall (which is in effect to consider the limit $G_s \to \infty$). This gave satisfactory results and agreement with a wide range of rigid-wall eigenvalues for $G_s/\rho \approx 20$. The basic numerical code has also been satisfactorily tested for the Orr–Sommerfeld/Blasius boundary-layer compliant problem against existing validated results.

5. Results

5.1. *Stationary modes*

The effect of wall compliance on the neutral curves for stationary disturbances is demonstrated in figure 2, where three different rotation rates have been considered. For these results and subsequently, until indicated otherwise, there is no wall damping, i.e. $\gamma_s = 0$, making the wall material purely elastic. The effect of rotation on the compliant wall is to change its effective compliance by variations in Ω if R remains fixed, whereas rigid-wall characteristics are unchanged. It can be seen that wall compliance has a stabilizing influence on the Type I eigenmodes with slight increases in the critical Reynolds number as the effective wall compliance is increased (higher rotation speeds). But, the effect on the stationary Type II eigenmode ($R_c = 440$ for the rigid wall) is more complex. For relatively low levels of wall compliance the effect is destabilizing and a striking feature is the enlarged region of instability corresponding to $\Omega = 20\ \mathrm{rad\,s^{-1}}$ where the critical Reynolds number has fallen to 177. However, the destabilizing influence on the Type II mode is not a consistent feature and as the degree of wall compliance is raised this unstable region shrinks and ultimately vanishes at $\Omega = 60\ \mathrm{rad\,s^{-1}}$.

When considering the effect of wall compliance it is perhaps more important to consider the growth rates. The most rapidly growing mode is likely to dominate and be the one detected in experiments, so how wall compliance affects the maximum growth rate is of significance. Figure 3 shows amplification curves for the stationary Type I instability with the disc rotating at $60\,\mathrm{rad\,s^{-1}}$ at four different values of Reynolds number. This demonstrates the full effect of the compliant boundary and indicates a substantial stabilizing influence with the maximum growth rate reduced by more than 50% of the corresponding rigid-wall value at $R = 600$.

Amplitude ratio (or gain) provides an even better indication of the effects of wall compliance and have been calculated using an e^N-type of calculation following the method of Mack (1985) where $-\alpha_i$ is integrated from a fixed Reynolds number of $R_0 = 250$ (not the critical) such that

$$\ln\left(\frac{A_1}{A_0}\right) = \int_{R_0}^{R_1} (-\alpha_i)\mathrm{d}R.$$

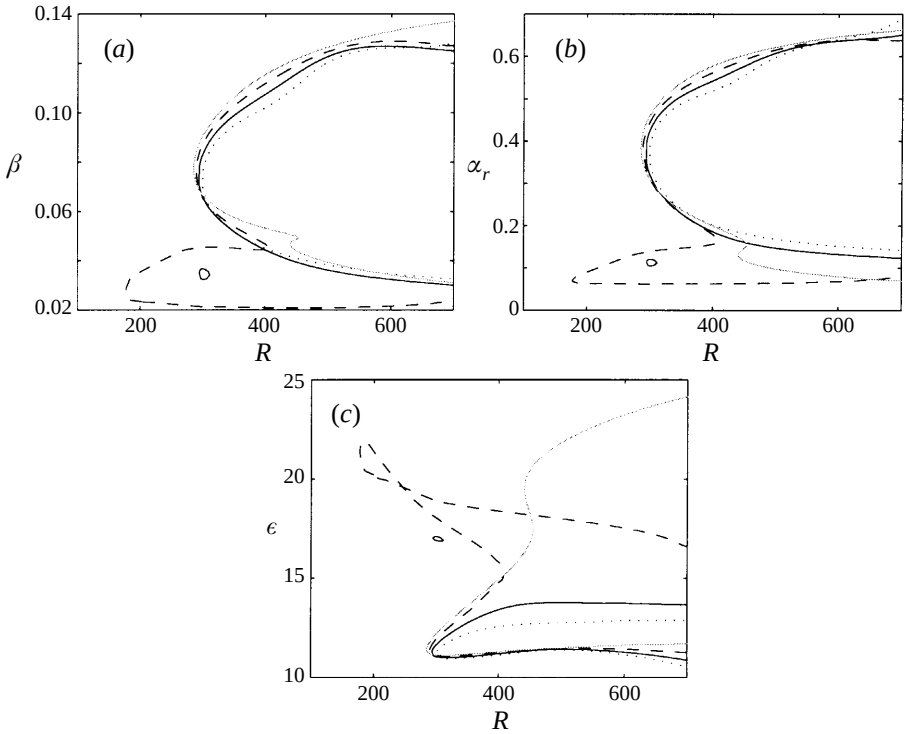

FIGURE 2. Neutral curves for stationary disturbances over rigid and compliant boundaries showing variation of R with (*a*) β, (*b*) α_r and (*c*) wave angle, $\varepsilon = \tan^{-1}(\beta/\alpha_r)$. Solid grey curve, rigid wall; compliant wall : - -, $\Omega = 20$ rad s^{-1}; —, $\Omega = 40$ rad s^{-1}; $\cdots$, $\Omega = 60$ rad s^{-1}.

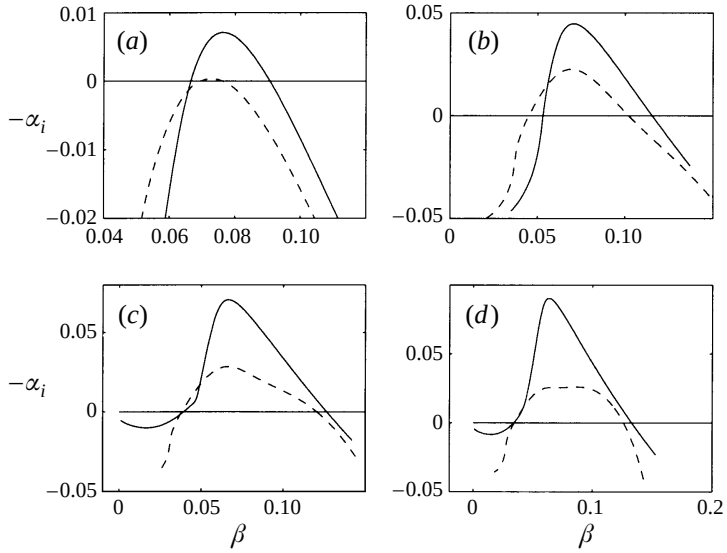

FIGURE 3. Amplification rates, $-\alpha_i$, for stationary Type I disturbances as a function of azimuthal wavenumber: —, rigid wall; - -, compliant wall, $\Omega = 60$ rad s^{-1}. (*a*) $R = 300$, (*b*) $R = 400$, (*c*) $R = 500$, (*d*) $R = 600$.

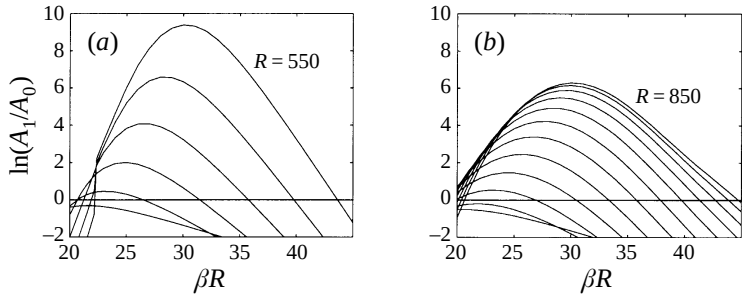

FIGURE 4. Amplitude ratios for the Type I stationary instability referenced to $R = 250$. (*a*) Rigid wall, (*b*) compliant wall, $\Omega = 60$ rad s^{-1}.

A_0 is the initial disturbance amplitude and A_1 the corresponding amplitude at R_1. The integration is performed under the condition of constant βR.

Previous e^N calculations for the rotating-disc boundary layer have been carried out by Malik *et al.* (1981), where spatial eigenvalues obtained from a group velocity transformation were integrated from a lower limit equal to the critical Reynolds number and calculations were based on a transitional Reynolds number of $R = 513$. They found that a factor of $N = 10.7$ corresponds to the transition location for the rigid disc. In their later improved experimental study (Wilkinson & Malik 1983, 1985) they concluded that the appropriate value of N lies between 9 and 10. For the compliant wall it is quite possible that the nonlinear regime of transition is radically different from the process over a rigid wall. Accordingly we have used a value of $N = 7$ in the present calculations, since this value corresponds approximately to the limit of the linear regime of transition in a low-noise environment. Thus when we use $N = 7$ to make comparisons of the amplitude ratios attained between rigid and compliant walls, it could be argued that we have not gone beyond the scope of our linear theory.

Differences in the calculation of the N-factor do not allow strict comparisons with the predictions of Malik *et al.* but the main point of this calculation is to compare results between rigid and compliant walls. Figure 4 shows amplitude ratio curves for (*a*) the rigid wall and (*b*) the compliant wall at $\Omega = 60$ rad s^{-1} starting at $R = 300$ and progressing in Reynolds number steps of 50. The labels in the figure refer to the Reynolds number of the outer amplification curve. It can be seen that the value of R at which $N \approx 7$ rises significantly to well above 850 when the compliant boundary is in place, suggesting that the reduced growth rates brought about by wall compliance also imply a delay in the onset of transition provided it occurs via the convective Type I instability.

5.2. *Energy equation*

An integral energy equation for three-dimensional disturbances, $[u, v, w, p]$, to an undisturbed three-dimensional boundary-layer velocity field, $[U, V, W]$, is derived in order to establish some underlying physical mechanisms behind the effect of the compliant boundary. The linearized momentum equations are multiplied by u, v and w respectively and summation of the combined equations, after some manipulation, gives rise to the following governing equation for the kinetic energy of

the disturbances:

$$\left\{\frac{\partial}{\partial t}+U\frac{\partial}{\partial r}+\frac{V}{r}\frac{\partial}{\partial\theta}+W\frac{\partial}{\partial z}\right\}K=-uw\frac{\partial U}{\partial z}-vw\frac{\partial V}{\partial z}-w^2\frac{\partial W}{\partial z}$$
$$-u^2\frac{\partial U}{\partial r}-\frac{Uv^2}{r}-\frac{1}{\rho}\left[\frac{\partial}{\partial r}(up)+\frac{1}{r}\frac{\partial}{\partial\theta}(vp)+\frac{\partial}{\partial z}(wp)+\frac{up}{r}\right]$$
$$+\frac{1}{\rho}\left[\frac{\partial}{\partial x_i}(u_j\sigma_{ij})-\sigma_{ij}\frac{\partial u_j}{\partial x_i}\right]+\nu\left[-\frac{u^2}{r}-\frac{2u}{r^2}\frac{\partial v}{\partial\theta}+\frac{2v}{r^2}\frac{\partial u}{\partial\theta}-\frac{v^2}{r^2}\right.$$
$$\left.+\frac{1}{r}\frac{\partial u}{\partial r}+\frac{1}{r}\frac{\partial v}{\partial r}+\frac{1}{r}\frac{\partial w}{\partial r}+\frac{1}{r}\left\{u\frac{\partial u}{\partial r}+\frac{v}{r}\frac{\partial u}{\partial\theta}+\frac{w}{r}\frac{\partial u}{\partial z}\right\}\right], \tag{45}$$

where σ_{ij} represents the viscous stress terms, repeated suffices indicate summation from 1 to 3 and $K=\frac{1}{2}(u^2+v^2+w^2)$.

By averaging the perturbations over a single period and aziumthal mode and integrating across the boundary layer, the derivatives with respect to t and θ, given real β, vanish to leave

$$\int_0^\infty \underbrace{\left[U\frac{\partial\overline{K}}{\partial r}\right]}_{\text{a}}+\underbrace{\frac{1}{\rho}\frac{\partial}{\partial r}(\overline{up})}_{\text{b}}-\underbrace{\frac{1}{\rho}\frac{\partial}{\partial r}\{\overline{u\sigma_{11}}+\overline{v\sigma_{12}}+\overline{w\sigma_{13}}\}}_{\text{c}}\Big]\,\mathrm{d}z$$
$$=\underbrace{\int_0^\infty\left[\left(-\overline{uw}\frac{\partial U}{\partial z}\right)+\left(-\overline{vw}\frac{\partial V}{\partial z}\right)+\left(-\overline{w^2}\frac{\partial W}{\partial z}\right)\right]\mathrm{d}z}_{\text{I}}-\underbrace{\frac{1}{\rho}\int_0^\infty\left(\overline{\sigma_{ij}\frac{\partial u_j}{\partial x_i}}\right)\mathrm{d}z}_{\text{II}}$$
$$-\underbrace{\frac{1}{\rho}\int_0^\infty\left(\frac{\overline{up}}{r}\right)\mathrm{d}z+\frac{1}{\rho}(\overline{wp})_{\mathrm{w}}}_{\text{III}}-\underbrace{\frac{1}{\rho}[\overline{u\sigma_{31}}+\overline{v\sigma_{32}}+\overline{w\sigma_{33}}]_{\mathrm{w}}}_{\text{IV}}$$
$$\underbrace{-\int_0^\infty W\frac{\partial\overline{K}}{\partial z}\mathrm{d}z-\int_0^\infty\overline{u^2}\frac{\partial U}{\partial r}\mathrm{d}z-\int_0^\infty\frac{U\overline{v^2}}{r}\mathrm{d}z}_{\text{V}}, \tag{46}$$

where overbars denote a period-averaged quantity, w subscripts denote quantities evaluated at the wall and $O(1/r)$ viscous terms have been dropped consistent with the neglect of $O(1/R^2)$ terms in the stability analysis.

Terms easily identified from the two-dimensional Cartesian version of this equation are the Reynolds stress production terms (I) and the viscous dissipation contribution (II). Term III contains pressure work terms where $(\overline{wp})_{\mathrm{w}}$ represents the work done by the fluctuating pressure on the wall and an additional pressure term arises from the use of the cylindrical coordinate system. Term IV describes the work done on the wall by the viscous stresses. The terms labelled V contains elements arising from streamline curvature effects and the three-dimensionality of the mean flow profile and have no corresponding two-dimensional Cartesian counterparts. In the energy analysis of Faller (1991) similar contributions were described as being dependent upon the geometrical effects of the change of R with radius (Rossby number terms). On the left-hand side there is the average disturbance kinetic energy convected by the radial mean flow component (a) followed by the work done by the perturbation pressure (b) and viscous stresses across some internal boundary in the fluid (c).

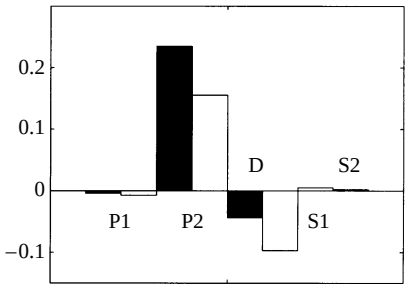

FIGURE 5. Comparison of numerical values between rigid and compliant contributions to terms in the energy balance equation at $R = 600$, $\omega = 0$. Unshaded regions correspond to compliant wall at $\Omega = 60\ \mathrm{rad\,s^{-1}}$ and shaded regions to rigid wall. P1 and P2: Reynolds stress production terms in radial and azimuthal directions respectively; D: viscous dissipation; S1 and S2: work done by viscous stresses at the wall in radial and azimuthal directions respectively.

The equation is subsequently normalized by the integrated mechanical energy flux so that

$$\begin{aligned} -2\alpha_i &= \text{normalized energy contributions} \\ &= (\mathrm{P1} + \mathrm{P2} + \mathrm{P3})(\mathrm{I}) + \mathrm{D}(\mathrm{II}) + (\mathrm{PW1{+}PW2})(\mathrm{III}) + (\mathrm{S1} + \mathrm{S2} + \mathrm{S3})(\mathrm{IV}) \\ &\quad + (\mathrm{G0} + \mathrm{G1} + \mathrm{G2})(\mathrm{V}) \end{aligned}$$

The notation for the constituent terms corresponds to the labelling in figures 5 and 8.

The energy calculation was carried out for the Type I instability at $R = 600$ and the various terms for the rigid wall and the compliant wall at $\Omega = 60\ \mathrm{rad\,s^{-1}}$ are compared for the most rapidly growing modes. Since the disturbances are stationary, the form of the compliant-wall boundary conditions implies that terms involving $w = \hat{h}\mathrm{e}^{\mathrm{i}(\alpha r + \beta R\theta - \omega t)} + \mathrm{c.c.}$ are identically zero. In the numerical calculations both sides of the energy equation are found to agree to at least three significant figures.

The constituent terms in the energy equation are compared in figure 5 where negligible terms have been omitted. The major influence of wall compliance is seen to occur through reductions to the rate of energy production by the Reynolds stresses and through an increase in conventional viscous dissipation. Work done by the viscous stresses at the wall plays a minor role with other terms negligible. Wall compliance therefore appears to have the same physical influence on this inviscid instability, in the way that growth rates are controlled, as it does on the viscous T–S instability.

5.3. *Travelling-wave modes*

The effect of wall compliance on non-stationary Type I modes is illustrated in figure 6 where maximum growth rate is plotted as a function of frequency. Negative values of frequency are taken to represent inwardly travelling disturbances, given that the wavenumber vector is restricted to point outwards in the direction of increasing radius. Wall compliance is seen to affect both the global maximum growth rate and the frequency range across which instability occurs. With increasing levels of wall compliance the maximum growth rate is reduced and moves to more positive frequencies with almost complete stabilization occurring at $\Omega = 60\ \mathrm{rad\,s^{-1}}$. No marked differences arise in terms of the radial wavenumber α_r at each β value so that as wall compliance is increased the value of β and the wave angle of the most rapidly growing mode are reduced. These observations are summarized in table 1.

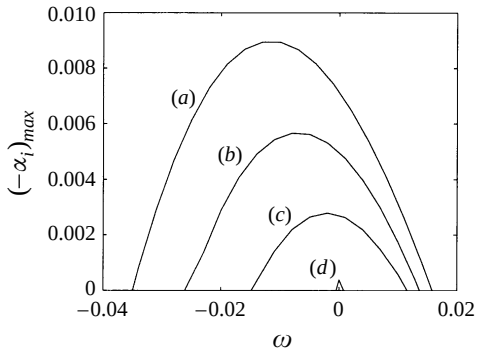

FIGURE 6. Effect of wall compliance on the maximum growth rate of the Type I disturbance across the unstable frequency range at $R = 300$. (*a*) Rigid wall; compliant wall: (*b*) $\Omega = 20$ rad s^{-1}; (*c*) $\Omega = 40$ rad s^{-1}; (*d*) $\Omega = 60$ rad s^{-1}.

Wall type	$(-\alpha_i)_{max}$	ω_{max}	β_{max}	ε_{max}
Rigid	0.0089395	−0.013	0.0980	15.37
Compliant: $\Omega = 20$ rad s^{-1}	0.0056594	−0.008	0.0890	13.61
Compliant: $\Omega = 40$ rad s^{-1}	0.0027896	−0.002	0.0765	11.85
Compliant: $\Omega = 60$ rad s^{-1}	0.0003852	0.000	0.0730	11.16

TABLE 1. Parameters giving maximum growth rate of Type 1 instability for travelling disturbances at $R = 300$. Subscript *max* refers to the position of maximum growth rate across the whole frequency range

Travelling Type II modes generally have a much lower critical Reynolds number than Type I travelling modes ($R_{cII} = 64.46$ compared to $R_{cI} = 283.6$, Balakumar & Malik 1990). Consequently unstable travelling Type II modes exist when the Type I disturbance is completely stable. Computations have been carried out at $R = 100$ and 200 for a disc rotation speed of $\Omega = 40$ rad s^{-1} in order to establish the effect of wall compliance on the travelling-wave Type II instability. Results are shown in figure 7 where maximum growth rate is plotted as a function of frequency. It can be seen that wall compliance is mildly destabilizing at $R = 100$ but the effect becomes more pronounced at $R = 200$, with a large departure from the general rigid-wall characteristics at the low-frequency end of the unstable range. Here frequencies which are completely stable for the rigid wall become strongly unstable in the presence of the compliant wall. The sharp peak in maximum growth rate evident in figure 7(*b*) marks a change in the character of the solution which is discussed in more detail later. Results from an energy balance calculation at one of these frequencies ($\omega = 0.0095$) are given in figure 8. This shows that the destabilization occurs through a large contribution to energy production from work done by viscous stresses at the wall, a component of the energy balance which is negligible in the results for the Type I instability. It is postulated that the large viscous stress work terms arise from the action of Coriolis forces in the system whereby motion perpendicular to the direction of propagation is induced resulting in large displacements at the interface. It should be noted that non-parallel effects are likely to be much stronger at these relatively low values of R and may well substantially modify the results discussed above

At higher Reynolds numbers the presence of a compliant boundary produces

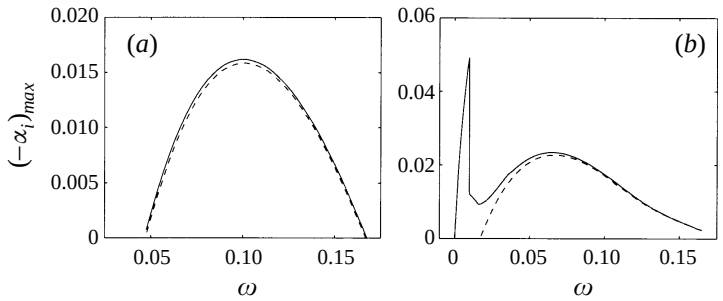

FIGURE 7. Effect of wall compliance on maximum growth rate of Type II disturbance across the unstable frequency range at (*a*) $R = 100$, (*b*) $R = 200$: - -, rigid wall; —, compliant wall at $\Omega = 40$ rad s^{-1}.

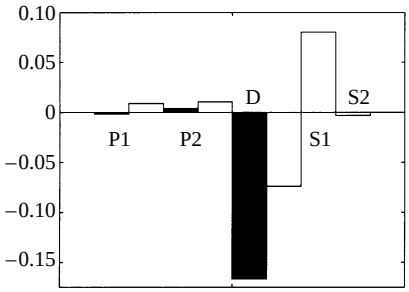

FIGURE 8. Energy budgets for Type II instability at $R = 200$, $\omega = 0.0095$, $\beta = 0.0125$. Unshaded regions correspond to compliant wall at $\Omega = 40$ rad s^{-1}. Notation as for figure 5.

more complex behaviour. This is apparent in figure 9 where at $R = 400$ a region of anomalous growth is evident for a range of values of β near zero which also correspond to a band of positive frequencies. It appears to be no coincidence that this irregular behaviour occurs in the ω–β range for which the Type I and II rigid-wall instabilities coexist and is similar to the type of behaviour in figure 7(*b*). This striking feature is found to persist at higher Reynolds numbers and rotation rates, but is completely eliminated when Coriolis and streamline curvature effects are neglected in the governing stability equations. The removal of these terms decouples the sixth-order system of equations and reduces the stability problem to that described by the Orr–Sommerfeld equation. The Type II mode is then effectively removed from the analysis since Coriolis effects are essential for its existence as an instability. The fact that removing the Type II instability eliminates the enlarged region of instability, plus the similarities with results for Type II at $R = 200$, suggest that the anomalous growth of instability is directly related to the destabilization of the Type II disturbance.

The physical effects of this strong destabilization can be revealed by considering flow and wall eigenfunctions and this may also possibly give some clues to help identify the mechanisms responsible. The eigenmode spectrum at $R = 400$ for $\omega = 0.004$ and $\Omega = 20$ rad s^{-1} is shown in figure 10. Eigenvalues corresponding to the stabilized Type I mode and the destabilized Type II mode are marked A and B respectively. Comparison of the compliant- and rigid-wall results reveals that the compliant-wall eigenmodes seem to exchange identities near the point where the two branches cross for the rigid wall. This is indicative of modal interaction. Flow eigenfunctions for eigenmodes A and B are illustrated in figure 11 and the change in the nature of the

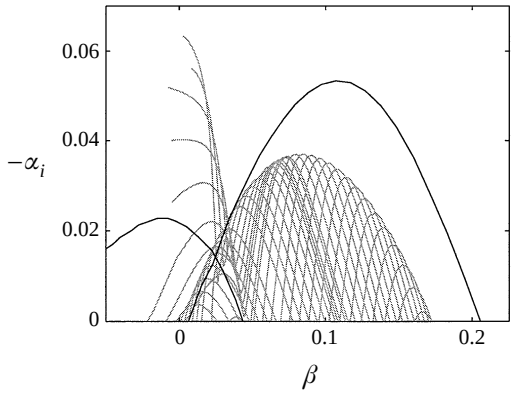

FIGURE 9. Amplification curves at $R = 400$. Grey lines indicate the amplification rate at a number of frequencies for the compliant wall at $\Omega = 20$ rad s^{-1}. Black lines indicate the rigid-wall maximum amplification envelopes.

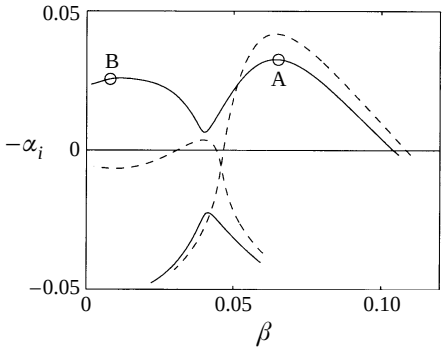

FIGURE 10. Eigenvalue spectrum at $R = 400$, $\omega = 0.004$ showing growth rate as a function of azimuthal wavenumber: - - , rigid wall branches; —, compliant wall, $\Omega = 20$ rad s^{-1}.

instability is clearly demonstrated. The maximum amplitude in both cases occurs with the azimuthal component of velocity but its position in the boundary layer and the general profiles are markedly changed. Large amplitudes are shown to occur exactly at the wall/flow interface for eigenmode B whereas for eigenmode A the main effect occurs some way into the boundary layer. The corresponding wall eigenfunctions are given in figure 12.

Figure 12 gives an indication of the validity of the assumption of an infinitely deep compliant wall. Figures 12(a, b) show that for the Type I instability the disturbance in the wall effectively disappears at a depth of $z \simeq 20$. For water ($\nu = 10^{-6}$ m^2 s^{-1}) and the given rotational speed $\Omega = 20$ rad s^{-1} this corresponds to a depth of less than 5 mm. The disturbances penetrate further in figure 12(c, d) for the Type II instability to about $z \simeq 50$ (i.e. about 11 mm). For our experimental programme the wall thickness is about 10 mm, so it would seem reasonable to regard the present results as a reliable guide to the behaviour of the instabilities in the experimental investigation.

The effect of wall damping on the Type I mode is demonstrated in figure 13(a). At $R = 300$ the frequency selected corresponds to the one which gives the maximum growth rate at $\Omega = 20$ rad s^{-1}. It is shown that increased levels of wall damping tend to be destabilizing which suggests that the Type I eigenmode is a Class A instability

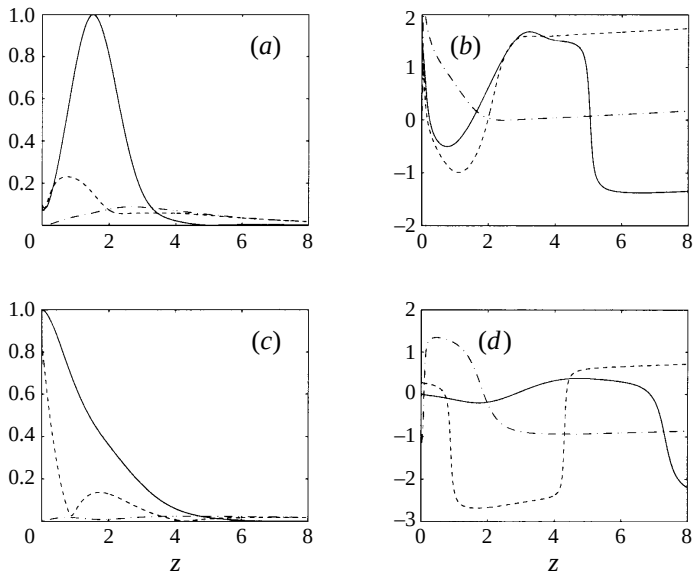

FIGURE 11. Flow eigenfunctions for compliant wall at $R = 400$, $\omega = 0.004$ and $\Omega = 20$ rad s^{-1}. Amplitudes and phase angles for eigenmode A are plotted in (*a*) and (*b*) respectively, and those for eigenmode B are plotted in (*c*) and (*d*) respectively. Amplitudes are normalized such that the maximum value is 1.0. Phase angles are plotted against an arbitrary origin. - -, f; —, g; — · —, h.

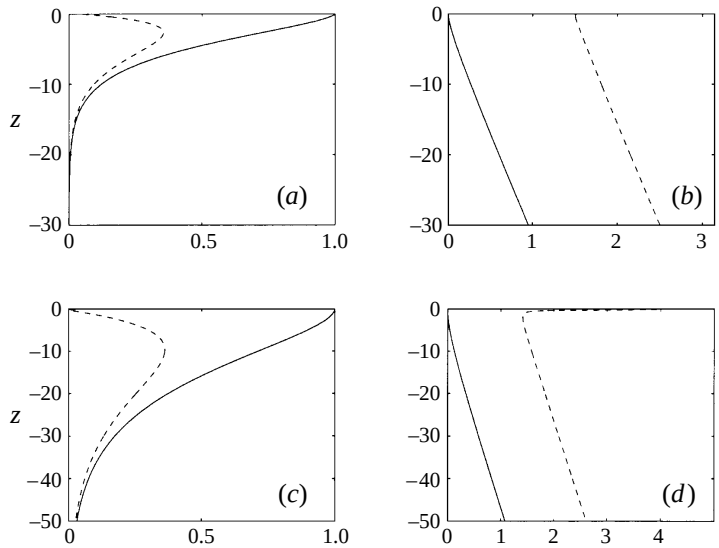

FIGURE 12. Wall eigenfunctions for compliant wall at $R = 400$, $\omega = 0.004$ and $\Omega = 20$ rad s^{-1}. Amplitudes and phase angles for eigenmode A are plotted in (*a*) and (*b*) respectively, and those for eigenmode B are plotted in (*c*) and (*d*) respectively. Amplitudes are normalized such that the maximum value is 1.0. Phase angles are plotted against an arbitrary origin. —, vertical displacement $\hat{\zeta}$; - -, horizontal displacement $\hat{\xi}\cos\varepsilon + \hat{\eta}\sin\varepsilon$.

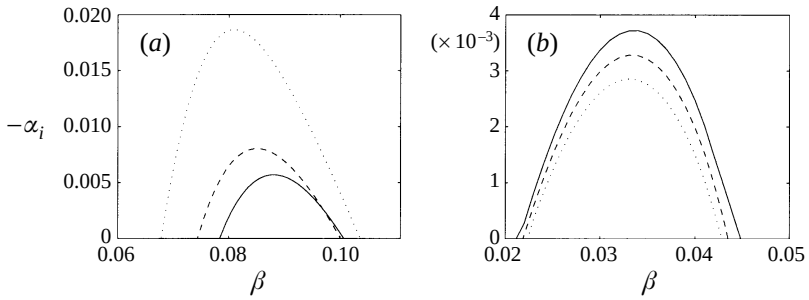

FIGURE 13. Change in growth rates with the inclusion of wall damping at $\Omega = 20$ rad s^{-1} for (*a*) Type I mode at $R = 300, \omega = -0.008$: —, undamped wall; - -, $\gamma_s = 0.0075$; $\cdots$, $\gamma_s = 0.0125$. (*b*) Type II mode at $R = 300, \omega = 0$: —, undamped wall; - -, $\gamma_s = 0.025$; $\cdots$, $\gamma_s = 0.05$.

(or negative energy wave) in the energy classification scheme of Benjamin (1960, 1963) and Landahl (1962). Figure 13(*b*) indicates that damping has a stabilizing influence on the Type II mode. This, together with the adverse reaction to wall compliance, defines it as a Class B instability (or positive energy wave). The fact that the Type I and II eigenmodes are of opposite energy type raises the possibility that they may well interact and coalesce. There is at least a hint of this occurring in figure 9. In fact, Lingwood (1995) in her figure 5 shows that there is a point of coalescence between the two eigenmodes at $R = 515$ even for the rigid wall. A similar phenomenon occurs for the Blasius boundary layer over a compliant wall when under the appropriate conditions the T–S waves can coalesce with the travelling wave flutter to form a powerful instability; see Carpenter & Garrad (1985), Sen & Arora (1988) and Carpenter (1990). The high amplification rates for the small positive values of β in figure 9 may well be evidence of something similar.

We investigated the conditions for the first occurrence of modal coalescence both for the rigid wall and for the compliant wall with $\Omega = 20$ rad s^{-1}. Illustrative results are plotted in figures 14 and 15. At the lower Reynolds numbers where coalescence first occurs $\alpha_i > 0$, i.e. the eigenmode is spatially stable. At higher values of R, α_i becomes negative at the point of coalescence. The conditions for which coalescence first occurs and for which the point of coalescence coincides with neutral stability are given in table 2 for both the rigid and compliant walls. It can be seen that modal coalescence occurs at a substantially lower value of R for the compliant wall than for the rigid surface. Including damping appears to postpone the appearance of coalescence to higher values of R or β depending on which parameter is fixed. This is reflected to some extent in figure 16. The approximate variation of α_i at the point of coalescence with R for the damped and undamped compliant wall is sketched in figure 17. Very extensive computational work would be required to produce an accurate version of figure 17.

What, then, is the significance of the modal coalescence? Figure 18 shows $-\alpha_i$ and the group velocity plotted against β for the conditions when coalescence first occurs for the compliant wall. (The group velocity is defined here as the real part of $\partial\omega/\partial\alpha$.) As would be expected the group velocity becomes zero at the point of coalescence. This suggests the possibility of an absolute instability. In order to verify the existence of absolute instability the pinch-point criterion of Briggs (1964) must be satisfied. Lingwood (1995, 1997) uses his approach to study the response of the rotating-disc boundary layer to impulsive excitation. The response is modelled as a double inverse Fourier transform with respect to complex ω $(= \omega_r + \mathrm{i}\omega_i)$ and complex α. In order

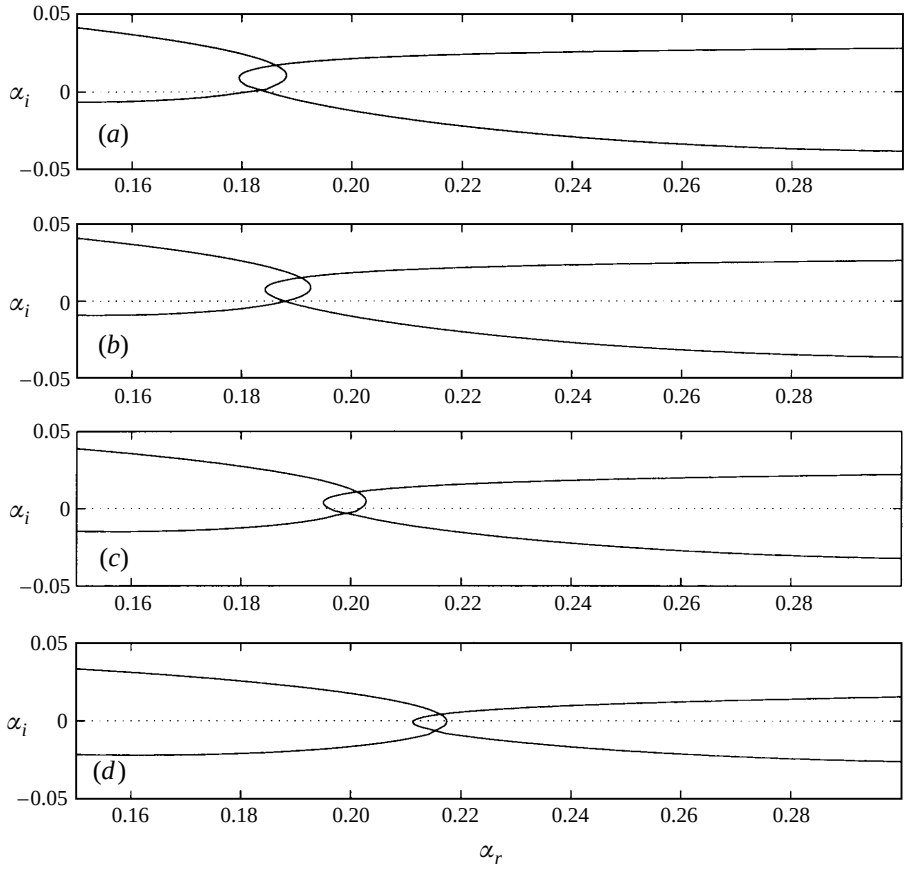

FIGURE 14. Spatial branches I and II in the α-plane ($\omega_i = 0$) for the rigid wall. (*a*) $R = 437$, $\beta = 0.041$; (*b*) $R = 439$, $\beta = 0.038$; (*c*) $R = 450$, $\beta = 0.030$; (*d*) $R = 500$, $\beta = 0.013$. Coalescence takes place at the lower of the two intersection points. The upper intersection point is an artifact of the projection of the branches from the (ω, α) space onto the α-plane.

to evaluate the Fourier transform the appropriate integration path in the complex α-plane must be chosen. The choice is made by initially choosing the value ω_i to be sufficiently large so as to exceed any possible temporal growth rates. ω_i is then progressively reduced to zero. When two poles, corresponding to eigenmodes, merge as ω_i is reduced there are two possible outcomes.

(i) If the two coalescing eigenmodes originate (at the initial value of ω_i) on opposite sides of the real axis in the α-plane then a pinch point forms where the corresponding poles merge and the integration path must move off the α_r-axis and pass through the pinch point. If $\omega_i > 0$ at the pinch point true temporal growth will occur implying absolute instability.

(ii) On the other hand if the poles originate in the same half of the α-plane a pinch point is not formed when they merge. ω_i can be reduced to zero and the integration path can be chosen to avoid the double pole; this can then be dealt with by means of the residue theorem. In this case true temporal growth does not occur implying it is not an absolute instability and, therefore, presumably convective.

Lingwood (1995, 1997) describes this procedure in detail. She shows that when Type I and III instabilities coalesce in the case of the rigid wall a pinch point is

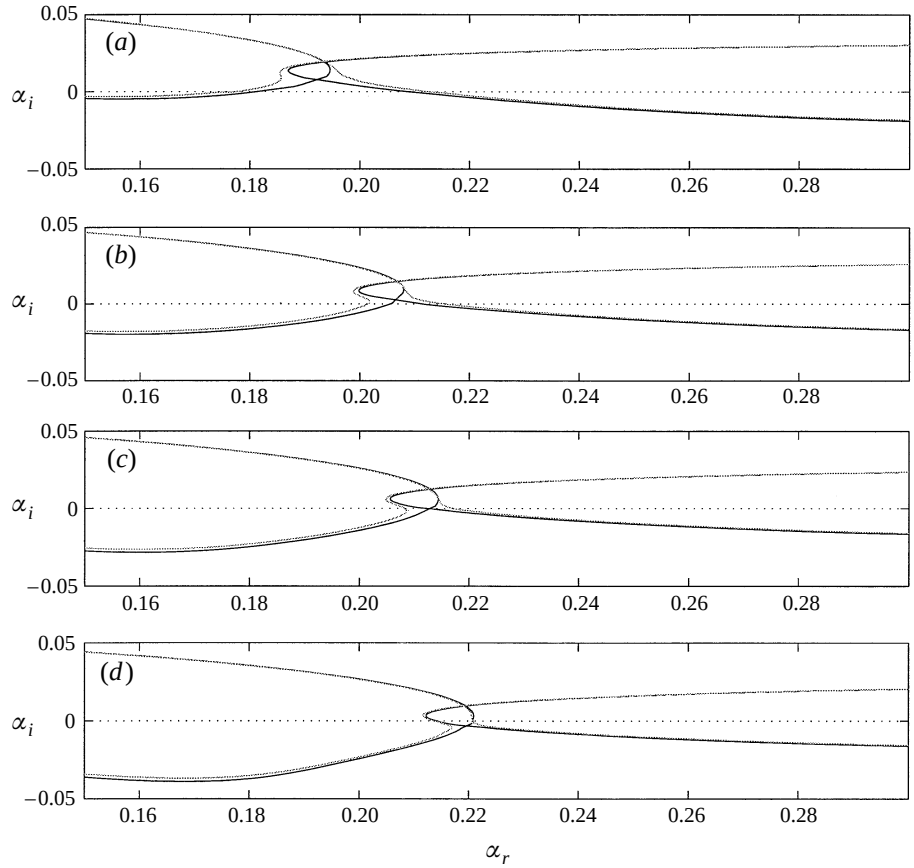

FIGURE 15. Spatial branches I and II in the α-plane ($\omega_i = 0$) for the compliant wall with $\Omega = 20$ rad s^{-1}. (*a*) $R = 373$, $\beta = 0.042$; (*b*) $R = 380$, $\beta = 0.035$; (*c*) $R = 387$, $\beta = 0.031$; (*d*) $R = 400$, $\beta = 0.025$. The black curves correspond to undamped walls and the grey curves to damped walls ($\gamma_s = 0.05$). Coalescence takes place at the lower of the two intersection points.

Wall type	α_r	α_i	ω	β	R
Rigid	0.185	0.0015	0.0061	0.041	437
Compliant: $\Omega = 20$ rad s^{-1}	0.188	0	0.00814	0.036	439
	0.193	0.0078	0.0047	0.042	373
	0.213	0	0.0132	0.031	387

TABLE 2. Parameters corresponding to the first appearance of the coalescence between the Type I and II eigenmodes and to it occurring at a point of neutral stability

formed. We find that this also occurs for a compliant wall. But even a relatively low level of wall compliance leads to a substantial rise in the critical Reynolds number for the absolute instability. This will be discussed in detail in Part 2 of the present paper. In the case of the coalescence of Type I and II instabilities, Lingwood shows that a pinch point does not form. We find that the use of a compliant wall does not alter this state of affairs. All that happens is that with wall compliance modal coalescence

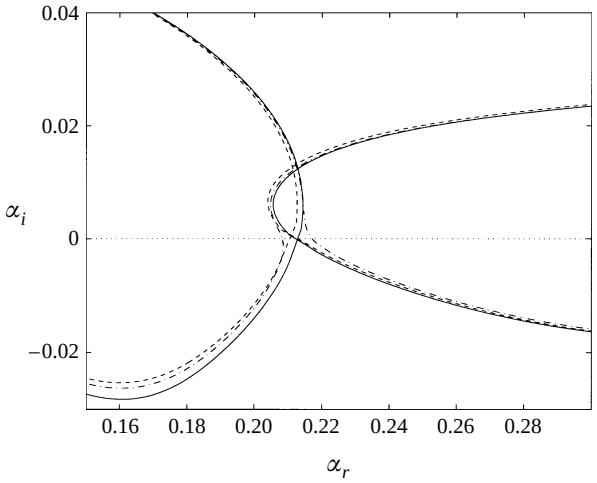

FIGURE 16. Expanded view of the spatial branches for the compliant wall with $\Omega = 20$ rad s^{-1} and $R = 387$ near the point of coalescence to show effects of damping and of slight variation in β: ——, $\beta = 0.0305$ (undamped); – · –, $\beta = 0.0305$ (damped); - - - , $\beta = 0.0308$ (damped). $\gamma_s = 0.05$ for damped walls. Coalescence takes place at the lower of the two intersection points.

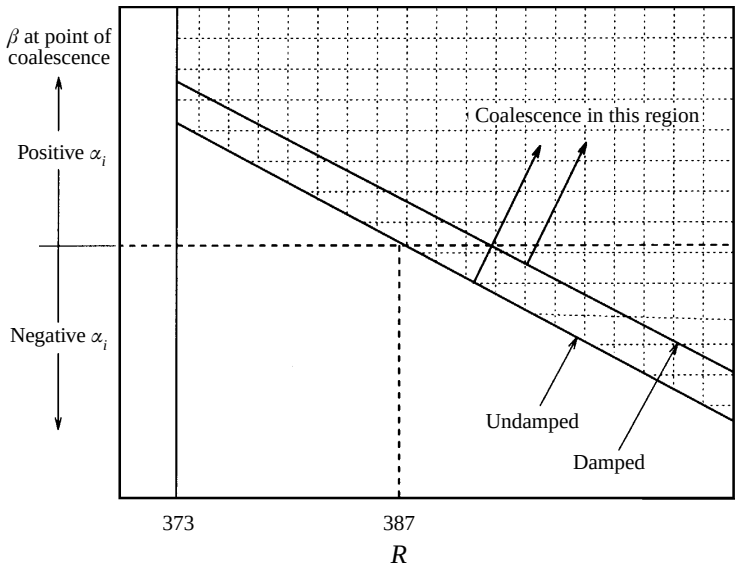

FIGURE 17. Sketch of the variation of α_i at the point of coalescence with R for damped and undamped compliant walls.

occurs at a lower Reynolds number. Note that this is precisely opposite to the effect of wall compliance on the absolute instability.

Does the second type of modal coalescence have any special significance? This question has been relatively little explored. It is not difficult to show from the residue theorem that terms of the form $r\exp\{\mathrm{i}(\alpha r + \beta R\theta - \omega_r t)\}$ appear when the Fourier integral is evaluated. Koch (1986) refers to this as *direct resonance* and investigates it in detail for the Orr–Sommerfeld equation. Terms of this form suggest the possibility of local algebraic growth even when the spatial growth rate is negative (i.e. $-\alpha_i < 0$)

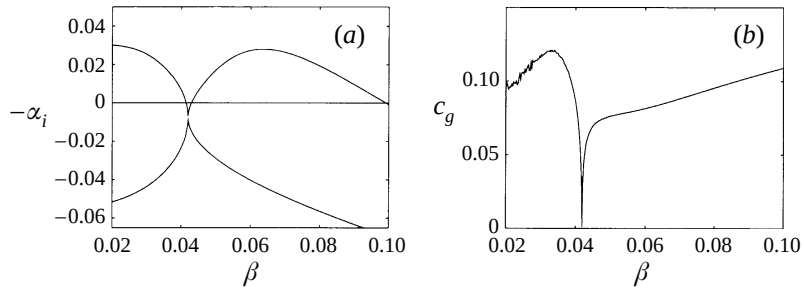

FIGURE 18. (*a*) Eigenmode structure and (*b*) group velocity for compliant wall at $R = 373$, $\omega = 0.00467$ and $\Omega = 20$ rad s^{-1}.

provided that the absolute value is fairly small. When the initial amplitude of the disturbance is large enough such algebraic growth can lead rapidly to nonlinear effects and provide another route to transition. Indeed Landahl and his co-workers (e.g. see Landahl 1980; Breuer & Haritonidis 1980; Breuer & Landahl 1990; Henningson, Lundbladh & Johansson 1993) have shown that local algebraic growth may well play a part in a possible by-pass transition mechanism.

6. Conclusions

The effect of an infinitely deep, single-layer, viscoelastic wall on instability in the rotating-disc boundary layer has been investigated.

In general this form of wall compliance is shown to increase the complexity of the eigenmode spectrum greatly and can have a significant stabilizing effect on the inviscid Type I instability. For stationary Type I disturbances instability growth rates and amplification rates at fixed Reynolds numbers are considerably reduced in value. The effect on amplitude ratio indicates a substantial increase in transitional Reynolds number if the Type I instability remains the route to transition. An analysis of the energy flux for this mode indicates that the stabilizing effect of the compliant boundary occurs through a reduction in energy production by the Reynolds shear stress and an increase in viscous dissipation.

The response of the viscous Type II mode to wall compliance is shown to be more complex. It is sensitive to rotation rate (i.e. to degree of wall compliance). For relatively low levels of wall compliance the effect is destabilizing whereas it becomes stabilizing for higher levels of compliance.

Travelling-wave modes have also been studied. At $R = 300$ both the overall amplification rate and the range of frequencies across which Type I instability occurs were successively reduced with increasing levels of wall compliance. However, it appears that wall compliance promotes a detrimental effect on the Type II instability leading to significantly large growth rates. A feature associated with this is the penetration of the boundary-layer disturbances to larger depths within the wall. The response of the Type I and II instabilities to wall damping identify them as negative and positive energy waves respectively. The co-existence of instabilities of opposite energy type suggests the possibility of modal coalescence. It is found that, compared with the rigid disc, wall compliance promotes modal coalescence. It is suggested that this may be associated with local algebraic growth, possibly hastening the onset of nonlinear effects.

For the type of wall studied in the present paper there is a significant degree

of freedom for horizontal motion. It may be that this makes the walls particularly vulnerable to the destabilization of the Type II eigenmode and the accompanying coalescence with the Type I mode. The addition of a thin, stiffer upper layer should act to constrain this horizontal motion and possibly suppress the destabilization of the Type II eigenmode. Results of direct numerical simulations by Davies & Carpenter (1995) (also reported in Carpenter 1997), using a spring-backed plate model for the compliant wall, appear to support this argument.

The work described in this paper was supported by research grants from EPSRC and MTD Ltd. The authors would also like to acknowledge useful discussions with Dr Rebecca Lingwood.

REFERENCES

Balachandar, S., Streett, C. L. & Malik, M. R. 1992 Secondary instability in rotating-disk flow. *J. Fluid Mech.* **242**, 323–347.

Balakumar, P. & Malik, M. R. 1990 Traveling disturbances in rotating-disk flow. *Theor. Comput. Fluid Dyn.* **2**, 125–137.

Bassom, A. P. & Gajjar, J. S. B. 1988 Non-stationary cross-flow vortices in three dimensional boundary-layer flows. *Proc. R. Soc. Lond.* A **417**, 179–212.

Benjamin, T. B. 1960 Effects of a flexible boundary on hydrodynamic stability. *J. Fluid Mech.* **9**, 513–532.

Benjamin, T. B. 1963 The three-fold classification of unstable disturbances in flexible surfaces bounding inviscid flows. *J. Fluid Mech.* **16**, 436–450.

Breuer, K. S. & Haritonidis, J. H. 1990 the evolution of a localized disturbance in a laminar boundary layer. Part 1. Weak disturbances. *J. Fluid Mech.* **220**, 569–594.

Breuer, K. S. & Landahl, M. T. 1990 the evolution of a localized disturbance in a laminar boundary layer. Part 2. Strong disturbances. *J. Fluid Mech.* **220**, 595–621.

Bridges, T. J. & Morris, P. J. 1984 Differential eigenvalue problems in which the parameter appears nonlinearly. *J. Comput. Phys.* **55**, 437–460.

Briggs, R. J. 1964 *Electron-Stream Interaction with Plasmas.* MIT Press.

Carpenter, P. W. 1990 Status of transition delay using compliant walls. In *Viscous Drag Reduction in Boundary Layers*, (ed. D. M. Bushnell & J. N. Hefner). Progress in Astronautics and Aeronautics, vol. 123, pp. 79–113. AIAA.

Carpenter, P. W. 1997 Current status of the use of wall compliance for laminar flow control. *Exp. Thermal Fluid Sci.*. (to appear).

Carpenter, P. W. & Cooper, A. J. 1996 Effect of wall compliance on rotating-disc boundary-layer stability. In *Proc. IUTAM Symp. on Nonlinear Instability and Transition in Three-Dimensional Boundary Layers* (eds. P.W. Duck & P. Hall), pp. 327–338. Kluwer.

Carpenter, P. W. & Garrad, A. D. 1985 The hydrodynamic stability of flows over Kramer-type compliant walls. Part 1. Tollmien–Schlichting instabilities. *J. Fluid Mech.* **155**, 465–510.

Chung, K. H. 1985 Composite compliant coatings for drag reduction utilising low modulus high damping silicone rubber. PhD Thesis, MIT.

Cooper, A. J. & Carpenter, P. W. 1995 The effects of wall compliance on instability in rotating disc flow. *AIAA Paper* 95-2257.

Cooper, A. J. & Carpenter, P. W. 1997*a* The effect of wall compliance on inflexion point instability in boundary layers. *Phys. Fluids* **9**, 468–470.

Cooper, A. J. & Carpenter, P. W. 1997*b* The stability of rotating-disc boundary-layer flow over a compliant wall. Part 2. Absolute instability. *J. Fluid Mech.* **350**, 261–270.

Corke, T. C. & Knasiak, K. F. 1996 Cross-flow instability with periodic distributed roughness. In *Proc. IUTAM Symp. on Nonlinear Instability and Transition in Three-Dimensional Boundary Layers* (ed. P. W. Duck & P. Hall), pp. 267-282. Kluwer.

Davies, C., & Carpenter, P. W. 1995 Novel velocity-vorticity formulation of the Navier–Stokes equations for boundary-layer disturbances. *Bull. Am. Phys. Soc.* **40**, 1956–1957.

Dixon, A. E., Lucey, A. D. & Carpenter, P. W. 1994 Optimization of viscoelastic compliant walls for transition delay. *AIAA J.* **32**, 256–267.

Faller, A. J. 1963 An experimental study of the instability of the laminar Ekman boundary layer. *J. Fluid Mech.* **15**, 560–576.

Faller, A. J. 1991 Instability and transition of the disturbed flow over a rotating disk. *J. Fluid Mech.* **230**, 245–269

Fedorov, B. I., Plavnik, G. Z., Prokhov, I. V. & Zhukhovitskii, L.G. 1976 Transitional flow conditions on a rotating disk. *J. Engng Phys.* **31**, 1448–1453.

Fraser, L. A. & Carpenter, P. W. 1985 A numerical investigation of hydroelastic and hydrodynamic instabilities in laminar flows over compliant surfaces comprising one or two layers of visco-elastic material. In *Numerical Methods in Laminar and Turbulent Flow*, pp. 1171–1181. Pineridge, Swansea, Wales, UK.

Gad-el-Hak, M. 1986 Boundary layer interactions with compliant coatings: An overview, *Appl. Mech. Rev.* **39**, 511–524.

Gaster, M. 1987 Is the dolphin a red herring? In *Proc. IUTAM Symp. on Turbulence Management & Relaminarisation, Bangalore, India* (ed. H. W. Liepmann & R. Narasimha), pp. 285–304. Springer.

Gregory, N., Stuart, J. T. & Walker, W. S. 1955 On the stability of three-dimensional boundary layers with application to the flow due to a rotating disk. *Phil. Trans. R. Soc. Lond.* A **248**, 155–199.

Hall, P. 1986 An asymptotic investigation of the stationary modes of instability of the boundary layer on a rotating disc. *Proc. R. Soc. Lond.* A **406**, 93–106.

Hansen, R. J. & Hunston, D. L. 1974 An experimental study of turbulent flows over compliant surfaces. *J. Sound Vib.* **34**, 297–308.

Hansen, R. J. & Hunston, D. L. 1976 Further observations on flow-generated surface waves in compliant surfaces. *J. Sound Vib.* **46**, 593–595.

Hansen, R. J. & Hunston, D. L. 1983 Fluid-property effects on flow-generated waves on a flexible surface. *J. Fluid Mech.* **133**, 161–177.

Henningson, D. S., Lundbladh, A. & Johansson, A. V. 1990 A mechanism for bypass transition from localized disturbances in wall-bounded shear flows. *J. Fluid Mech.* **250**, 169–207.

Jarre, S., Le Gal, P. & Chauve, M. P. 1991 Experimental analysis of the instability of the boundary layer over a rotating disk. *Europhys. Lett.* **14**, 649–654.

Jarre, S., Le Gal, P. & Chauve, M. P. 1996*a* Experimental study of rotating disk instability. I. Natural flow. *Phys. Fluids* **8**, 496–508.

Jarre, S., Le Gal, P. & Chauve, M. P. 1996*b* Experimental study of rotating disk instability. II. Forced flow. *Phys. Fluids* **8**, 2985–2994.

Kármán, Th. von 1921 Uber laminare und turbulente Reibung. *Z. Angew. Math. Mech.* **1**, 233–252.

Koch, W. 1986 Direct resonance in Orr-Sommerfeld problems. *Acta Mechanica* **58**, 11–29.

Kohama, Y. 1984 Study on boundary layer transition of a rotating disk. *Acta Mechanica* **50**, 193–199.

Kohama, Y. 1987 Crossflow instability in a rotating disk boundary layer. *AIAA Paper* 87-1340.

Kohama, Y. & Suda, K. 1993 Crossflow instability in a spinning disk boundary layer. *AIAA J.* **31**, 211–214.

Landahl, M. T. 1962 On the stability of a laminar incompressible boundary layer over a flexible surface. *J. Fluid Mech.* **13**, 609–632.

Landahl, M. T. 1980 A note on an algebraic instability of inviscid parallel shear flow. *J. Fluid Mech.* **98**, 243–251.

Le Gal, P. 1992 Complex demodulation applied to the transition to turbulence of the flow over a rotating disk. *Phys. Fluids* A **4**, 2523–2528.

Lilly, D. K. 1966 On the instability of Ekman boundary flow. *J. Atmos. Sci.* **23**, 481–494.

Lingwood, R. J. 1995 Absolute instability of the boundary layer on a rotating disk. *J. Fluid Mech.* **299**, 17–33.

Lingwood, R. J. 1996 An experimental study of absolute instability of the rotating-disk boundary-layer flow. *J. Fluid Mech.* **314**, 373–405.

Lingwood, R. J. 1997 On the application of the Briggs' and steepest-descent methods to a boundary-layer flow. *Stud. Appl. Maths* **98**, 213–254.

Lucey, A. D. & Carpenter, P. W. 1995 Boundary layer instability over compliant wall : Comparison between theory and experiment. *Phys. Fluids* **7**, 2353–2363.

MACK, L. M. 1985 The wave pattern produced by point source on a rotating disk. *AIAA Paper* 85-0490.

MACKERRELL, S. O. 1987 A nonlinear, asymptotic investigation of the stationary modes of instability of the three-dimensional boundary layer on a rotating disc. *Proc. R. Soc. Lond.* A **413**, 497–513.

MALIK, M. R. 1986 The neutral curve for stationary disturbances in rotating disk flow. *J. Fluid Mech.* **164**, 275–287.

MALIK, M. R., WILKINSON, S. P. & ORSZAG, S. A. 1981 Instability and transition in rotating disk flow. *AIAA J.* **19**, 1131–1138.

RAYLEIGH, Lord 1880 On the stability, or instability, of certain fluid motions. *Proc. Lond. Math. Soc.* **11**, 57–70.

RILEY, J. J., GAD-EL-HAK, M. & METCALFE, R. W. 1988 Compliant coatings. *Ann. Rev. Fluid Mech.* **20**, 393–420.

SEN, P. K & ARORA, D. S. 1988 On the stability of laminar boundary-layer flow over a flat-plate with a compliant surface. *J. Fluid Mech.* **197**, 201–240.

SMITH, N. H. 1946 Exploratory investigation of laminar-boundary-layer oscillations on a rotating disk. *NACA TN* 1227.

WILKINSON, S. P. & MALIK, M. R. 1983 Stability experiments in rotating-disk flow. *AIAA Paper* 83-1760.

WILKINSON, S. P. & MALIK, M. R. 1985 Stability experiments in the flow over a rotating disk. *AIAA J.* **23**, 588–595.

YEO, K. S. 1988 The stability of boundary layer flow over single- and multi-layer viscoelastic walls. *J. Fluid Mech.* **196**, 359–408.

YEO, K. S., KHOO, B. C. & CHONG, W. K. 1994*a* The linear-stability of boundary-layer flow over compliant walls – effects of boundary-layer growth. *J. Fluid Mech.* **280**, 199–225.

YEO, K. S., KHOO, B. C. & CHONG, W. K. 1994*b* The linear-stability of boundary-layer flow over compliant walls – the effects of the wall mean state, induced by fluid loading. *J. Fluids Struc.* **8**, 529–551.